Mixed DEM/FEM Modeling of Advanced Damage in Reinforced Concrete Structures

Serguei Potapov[1]; Aurélien Masurel[2]; Philippe Marin[3]; and Laurent Daudeville[4]

Abstract: This paper aims to present a mixed, or combined, numerical approach to modeling advanced degradation and predicting failure in reinforced concrete (RC) structures. The discrete-element method (DEM) is used to model the cohesive behavior and fracturing of concrete, whereas the standard finite-element method (FEM) is applied to represent steel reinforcement through an elastic-plastic beam model. Because of specificity in the geometric support, which does not allow for hierarchical mesh refinement, convergence of the spherical DEM has never been proved, making it difficult to master DE simulations. In this paper the authors present results of a computational study conducted by means of deforming a DEM sample and varying several parameters, which allowed determining the minimum discretization required for a DEM sample to correctly reproduce the macroscopic behavior of concrete, and thus evaluating consistency of the spherical DEM used herein. An original steel-concrete bond model, developed to simulate the interaction between the steel and concrete models, is also presented. This model was devised to decouple normal and tangential responses, which allows fitting them separately in accordance with experimental data. The numerical simulations of tests performed on unreinforced and reinforced concrete samples and the modeling of the hard-type impact on a RC beam indicate the relevance of the proposed approach for simulating advanced damage in civil engineering structures under both static and dynamic loads. **DOI: 10.1061/(ASCE)EM.1943-7889.0001173.** *© 2016 American Society of Civil Engineers.*

Author keywords: Reinforced concrete; Discrete-element method (DEM); Damage; Steel-concrete bond model.

Introduction

The discrete-element method (DEM) is a powerful alternative to the finite-element method (FEM) whenever advanced damage states and concrete failure need to be studied (Camborde et al. 2000; Hentz et al. 2004a). Although continuous approaches such as FEM are well adapted to the nonlinear analysis of structures before failure, their limitations are exposed when seeking to describe macrocracking and fragmentation mechanisms. The use of erosion techniques (Belytschko and Lin 1987) may generate discontinuities in the standard FEM, but the full algorithm becomes difficult to control during the fragmentation process (due to difficulties of mass and energy conservation and contact treatment of newly created surfaces); moreover, results are entirely dependent on the erosion criterion applied.

To overcome the difficulty of FEM in describing large material deformations and material discontinuities, many so-called meshfree methods have been developed—smooth particle hydrodynamics (SPH), element free Galerkin (EFG), reproducing kernel particle method (RKPM), material point method (MPM), meshless local Petrov–Galerkin (MLPG), and so forth (see Nguyen et al. 2008; Liu 2010 for a review)—using either strong or weak formulation of equations, global or local background mesh to perform integration, and different definitions of the support domain and shape functions if used. In contrast, DEM is a completely discontinuous approach to representing the material; thus, it does not need any background integration mesh. Particles-based (Camborde et al. 2000; Hentz et al. 2004a), lattice-based (Prado and Van Mier 2003), and mixed lattice discrete particle models (Cusatis et al. 2011) have been proposed to study fracturing in rocks and plain concrete on different micro-, meso-, or macroscopic modeling scales. DEM easily yields realistic (from a qualitative standpoint) macrocrack patterns and material fragments given its discontinuous nature. Yet it must still be handled carefully with regard to calibration of its parameters and mesh construction in order to produce physically (quantitatively) realistic results.

Most real concrete engineering structures are strengthened by ribbed steel rods called reinforcing bars, or rebars, to ensure structural resistance in regions where high tensile stresses appear and the concrete is cracked. For the numerical model to accurately predict the advanced degradation states and failure of reinforced concrete, two key modeling components must be developed and duly validated: the plain concrete model and the steel-concrete bond model. Both are discussed within the computational framework set forth herein.

To begin, a brief theoretical description of the spherical-type DEM, adopted here to model concrete behavior on a macroscopic level, is presented. Because of specificity in the geometric support, which does not allow for hierarchical mesh refinement, it is not possible to mathematically prove convergence of the considered DEM. The only way to prove the credibility of the spherical DEM approach is to simulate a variety of existing experiments involving different loading conditions, different sizes and forms of specimens, and going from elementary plain concrete samples to industrial-type reinforced concrete structures. Moreover, mastering calculations using spherical DEM requires answering two important questions: (1) what is the minimum fineness of the discrete-element

[1]Senior Research Scientist, EDF-CNRS-CEA-ENSTA IMSIA, UMR 9219, 1 Av. du Général-de-Gaulle, 92141 Clamart Cedex, France (corresponding author). E-mail: serguei.potapov@edf.fr

[2]Ph.D. Student, EDF-CNRS-CEA-ENSTA IMSIA, UMR 9219, 1 Av. du Général-de-Gaulle, 92141 Clamart Cedex, France. E-mail: au.masurel@gmail.com

[3]Associate Professor, CNRS 3SR UMR 5521, Univ. of Grenoble Alpes, F-38000 Grenoble, France. E-mail: philippe_marin@yahoo.fr

[4]Professor, CNRS 3SR UMR 5521, Univ. of Grenoble Alpes, F-38000 Grenoble, France. E-mail: laurent.daudeville@ujf-grenoble.fr

Note. This manuscript was submitted on October 2, 2015; approved on August 5, 2016; published online on October 28, 2016. Discussion period open until March 28, 2017; separate discussions must be submitted for individual papers. This paper is part of the ***Journal of Engineering Mechanics***, © ASCE, ISSN 0733-9399.

(DE) assembly needed in order to guarantee that the DEM accurately reproduces the macroscopic behavior of the material under various types of loading; (2) how do DE assembly properties (fineness, compactness) and packing method influence DEM model behavior? To answer these questions and obtain information on the consistency of the DEM model employed, an extensive computational study was conducted by varying DE mesh fineness and compactness when subjecting DE samples to compressive and shear loads. The main results from this study as well as from two DE simulations of well-known tests (i.e., the Brazilian indirect splitting test and Nooru-Mohamed's shear-tension test on a double-edge notched specimen) are presented to demonstrate the capability of the DEM model introduced to reproduce crack initiation and propagation in a multiaxial case.

Next, a new steel-concrete bond model is presented in order to appropriately tie FEM rebar to DEM concrete. This model decouples the normal and tangential responses of the steel-concrete interface and moreover allows choosing a suitable form of the constitutive laws for each component. The two methods can therefore be fitted separately in accordance with experimental data. The normal and tangential bond laws are also described.

To illustrate the modeling capabilities of this proposed mixed DEM/FEM approach, as implemented in the *EUROPLEXUS* fast dynamics software, the simulation of a steel-concrete tie in tension and the hard-type impact on a RC beam are presented and analyzed.

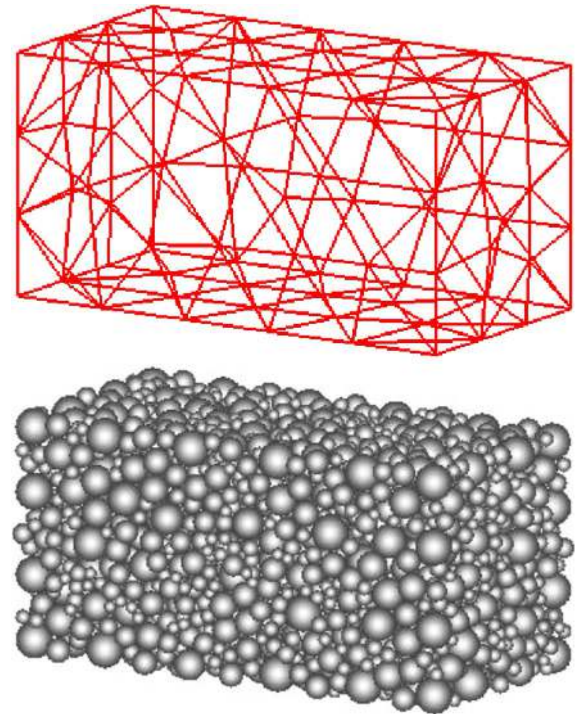

Fig. 1. Initial tetrahedral mesh and the resulting DE mesh

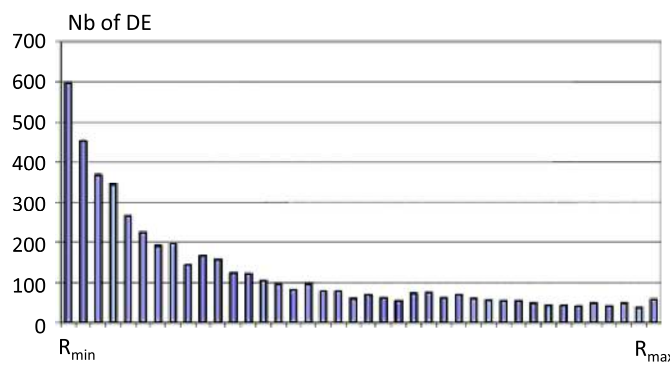

Fig. 2. Typical DE size distribution in a DE sample

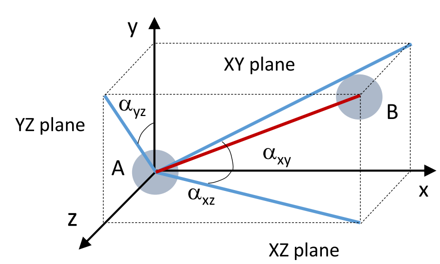

Fig. 3. Main planes for the projection of links in a DE sample

Discrete-Element Modeling of Concrete

General Presentation of the Discrete-Element Model

The DEM considered herein corresponds to the descriptions provided in Hentz et al. (2004b) and Rousseau et al. (2008, 2009). The DEM is based on cohesive and contact interactions linking discrete elements. Discrete elements are rigid spheres of different sizes and masses. DE mesh constitutes a disordered polydisperse assembly generated by a special geometric algorithm (Jerier et al. 2010) that allows padding (filling) a given tetrahedral mesh of the modeled structure using spheres of varying sizes. To illustrate this, Fig. 1 shows an initial tetrahedral mesh of a rectangular sample and the resulting DE mesh. This padding algorithm was implemented in the *SpherePadder++* free software, which was subsequently introduced as a plug-in module into the open-source *SALOME* platform. The *SpherePadder++* algorithm yields a very regular DE size distribution (as depicted in Fig. 2) between the minimum and maximum radii imposed by the user.

The characteristic size of the discrete elements used herein is not representative of concrete constituents such as aggregates. In fact, this model is of a higher scale and seeks to reproduce the macroscopic behavior of concrete in both linear and nonlinear regimes. The behavior of undamaged plain concrete is assumed to be linear, elastic, isotropic, and homogeneous. The discrete-element assembly is thus required to be isotropic so as to reproduce the isotropic property of undamaged concrete and prevent the development of nonphysical cleavage, which may appear with aligned elements when the concrete behavior becomes nonlinear. In a DEM context, the isotropy of a DE assembly can be evaluated by projecting contact orientations onto three orthogonal planes. Fig. 3 shows angles (α) used to project a link between two discrete elements denoted A and B (Fig. 3).

To evaluate the isotropic property of DEM meshes, a parallelepiped sample was first meshed with increasingly refined tetrahedral meshes, containing between 1 and 9 tetrahedra per transverse edge, and then transformed by *SpherePadder++* into DE assemblies with different levels of fineness. For all DE meshes, the following ratios were used (default options set for *SpherePadder++*): $R_{\max}/R_{\min} = 3$ and FE tetrahedron edge/DE mean diameter = 4. The DE meshes obtained and the rosette projections for one of the mesh generators employed are shown in Fig. 4. As can be observed, DEM model isotropy is quickly established as the mesh becomes more refined. As an example, for Sample 4, derived from the tetrahedral mesh containing 4 tetrahedra per edge,

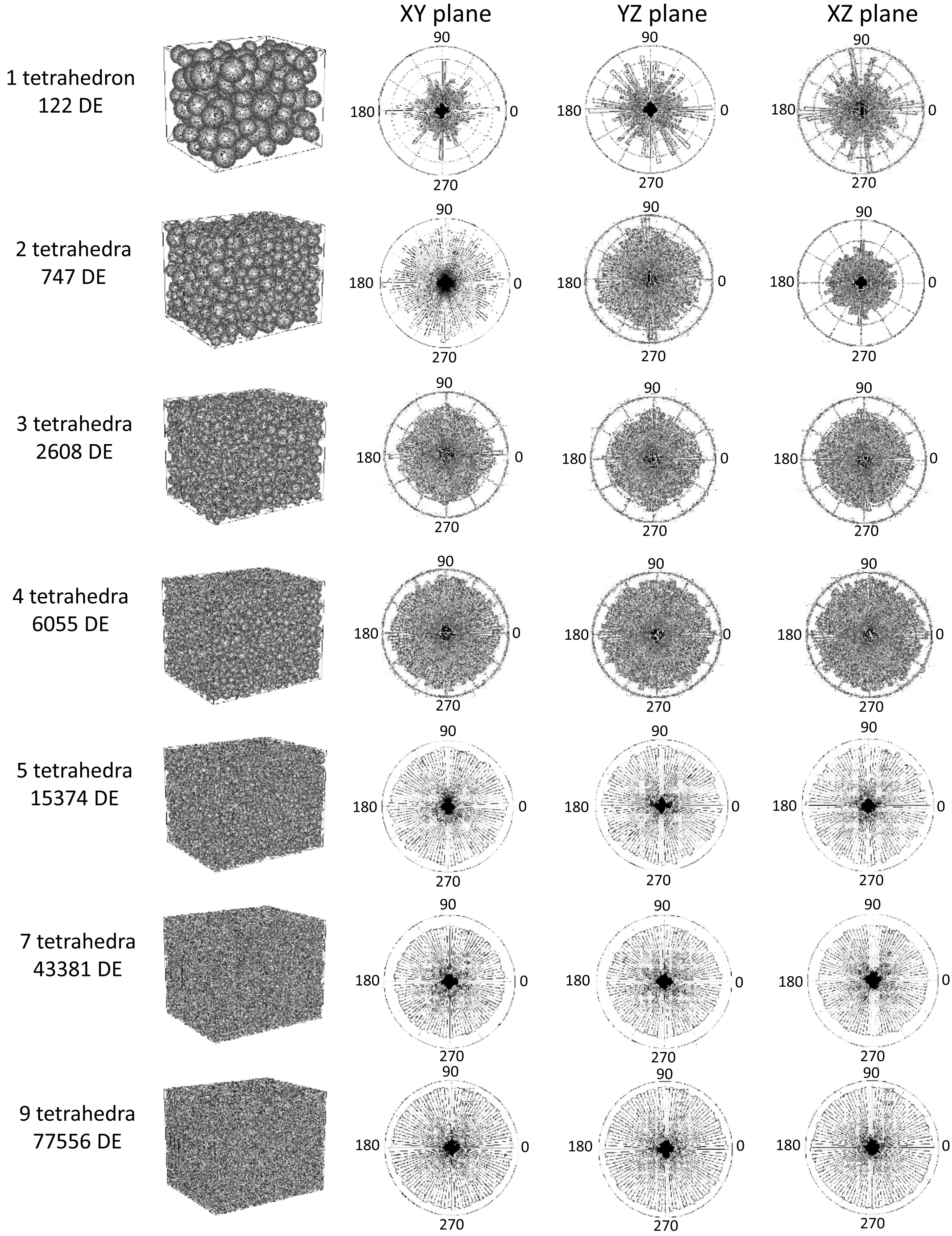

Fig. 4. DE sample meshes and distribution of contact orientations in the XY, YZ, and XZ planes

the interaction distribution is nearly uniform; hence, the sample can be assumed to exhibit isotropic behavior.

Linear Elastic Cohesive-Type Model

Apart from its initial isotropy, the cohesive-type DE model needs to reproduce the macroscopic elastic behavior of the solid material volume under various loading conditions. Because the DE model considered herein is a complex mass-spring system governed by Newton's laws and does not satisfy continuum mechanics equations, as opposed to FEM, the aforementioned requirement is not automatically met. Local DEM properties must therefore be identified by comparing the DEM response in tension and compression with the corresponding laboratory tests. In other words, local model parameters are calibrated to enable DEM to reproduce macroscopic concrete behavior.

Cohesion-type interactions in each pair of neighboring discrete elements are defined by means of nonlinear normal and tangential (shear) stiffnesses. Because the strain energy for a given cohesive spring-type link depends on the size of the interacting elements, the local interaction stiffnesses are not identical throughout the sample. *Micro-macro* relations (see Hentz et al. 2004b for details) are used to calculate these local stiffnesses K_N and K_S in the elastic regime from macroscopic elastic parameters—namely, Young's modulus E and Poisson's ratio ν:

$$K_N = \frac{ES_{\rm int}}{D_{IJ}} \frac{1+\alpha}{\beta(1+\nu)+\gamma(1-\alpha\nu)}$$

$$K_S = K_N \frac{1-\alpha\nu}{1+\nu} \tag{1}$$

where $S_{\rm int} = \min(\pi R_I^2, \pi R_J^2)$ = interaction surface for a pair of interacting discrete elements I and J; D_{IJ} = distance between their centers; and α, β, and γ = set of parameters specific to the packing algorithm.

The relations in Eq. (1) stem from homogenization models adapted to take into account both the relative disorder of the DE assembly and the dependence of the interaction surface on the size of the interacting elements. After calibration, therefore, the local parameters α, β, and γ of the DE model account for the size and spatial distribution of discrete elements in the sample; moreover, they are a priori specific to each packing algorithm. To enable the DEM to correctly reproduce the cohesive features and initial isotropy of concrete, cohesive links must interconnect the discrete elements beyond their immediate neighbors. All details about parameter identification (i.e., general procedure, order of identification, choice of the form and size of samples, etc.) can be found in Rousseau (2009).

Consistency Study of the Model in the Elastic Regime

As opposed to FEM, whose convergence properties are well established with increased mesh refinement, it is not possible to prove convergence for the spherical DEM used herein because it does not lead to hierarchical mesh refinement. Every modification of the DE mesh thus involves a change in its *properties*, requiring, strictly speaking, a recalibration of local parameters. To guarantee the quality of DEM calculations, two important questions first need to be answered: (1) what is the minimum level of fineness of the DE assembly required in order to ensure that the DE model is accurately reproducing the macroscopic behavior of the material under various types of loadings and (2) how do DE assembly properties (fineness, compactness) and packing method influence the DEM model response?

To obtain information on the consistency of the spherical DEM model, the authors conducted an extensive computational study whereby DE samples of different fineness, compactness, and geometry were subjected to quasi-static compressive and shear loads. In this study, the local parameters of micro-macro relations [Eq. (1)] were identified on Sample 4 (i.e., with 4 tetrahedra per edge) when simulating a compression test by imposing an increasing axial displacement on discrete elements located in the vicinity of the sample's opposite ends. This set of parameters was subsequently used for the other samples when simulating the uniaxial compression test. The mean values of Young's modulus (E) and Poisson's ratio (ν) were then determined from the deformed state of the samples and reported in Fig. 5. Table 1 summarizes relative errors between the reproduced and the target values of E and ν obtained for different DE meshes. It can be observed that for Sample 4 (i.e., the one used for local parameter identification), the values of global parameters E and ν are replicated almost identically. When applying the same set of local parameters to finer-meshed samples, results do not vary considerably: the maximum error obtained for

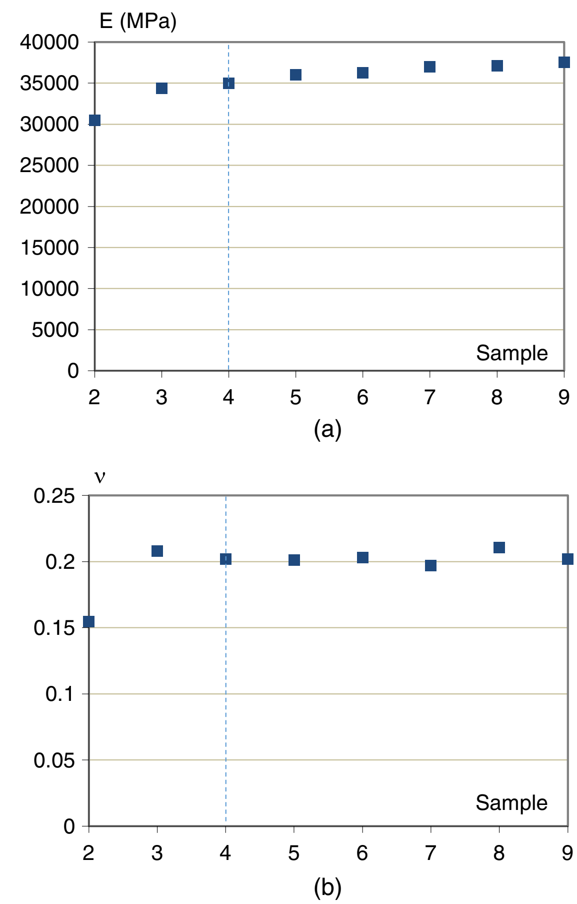

Fig. 5. Reproducibility of (a) Young's modulus and (b) Poisson's ratio values for various sample DE meshes

Table 1. Relative Errors on Young's Modulus and Poisson's Ratio Values

Sample	Error on Young's modulus (%)	Error on Poisson's ratio (%)
2	13.1	22.5
3	1.8	4.1
4	0.1	1.1
5	2.8	0.7
6	3.7	1.5
7	5.6	1.4
8	6.0	5.3
9	7.2	1.1

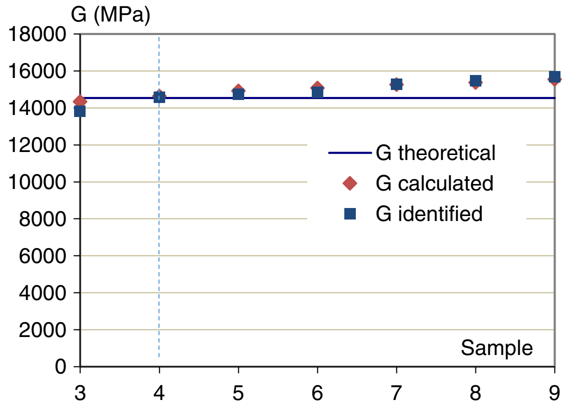

Fig. 6. Reproducibility of the shear modulus for various sample DE meshes

Table 2. Errors on the Shear Modulus

Sample	G (GPa) calculated	Error (%)	G (GPa) observed	Error (%)
3	14.34	1.4	13.82	4.9
4	14.63	0.6	14.58	0.3
5	14.92	2.6	14.74	1.4
6	15.07	3.7	14.85	2.2
7	15.26	4.9	15.28	5.1
8	15.36	5.7	15.45	6.3
9	15.55	6.9	15.67	7.8

E and ν does not exceed 8% in the worst case (Table 1), which attests to some consistency of the spherical DEM model and suggests the possibility of reusing the same set of parameters for different discretizations, provided they are produced with the same tetra-mesh generator, thus avoiding the systematic recalibration of local parameters. However, the use of finer meshes with the parameters calibrated on a coarse mesh can lead to overestimating the resistance capacity of the structure.

Very similar results were obtained when simulating a pure shear test using a cubic-shaped sample (Fig. 6 and Table 2). In this case, two computed values of shear modulus G were compared with the theoretical G value: the first one was identified from the deformed sample dimensions and applied force, whereas the second was calculated from the Young's modulus and Poisson's ratio values previously identified for the considered samples (Fig. 5).

The results obtained clearly indicate the minimum discretization needed for a DE sample to reproduce the macroscopic behavior of the material for both compression and shear types of loadings. The mesh fineness derived for Sample 4 (with 4 tetrahedra per edge) seems to be a good compromise between precision and cost, whereas coarser meshes would obviously be insufficient and should not be used. Finer meshes should be used whenever a complex crack pattern is foreseen in the concrete.

Identification and Validation of the Nonlinear Constitutive Model for Concrete

The nonlinear behavior of concrete is modeled by means of two local rupture criteria:

$$f_1(F_n, F_s) = F_s - \tan(\Phi_i)F_n - S_{\text{int}}C_o \tag{2}$$

$$f_2(F_n, F_s) = S_{\text{int}}T - F_n \tag{3}$$

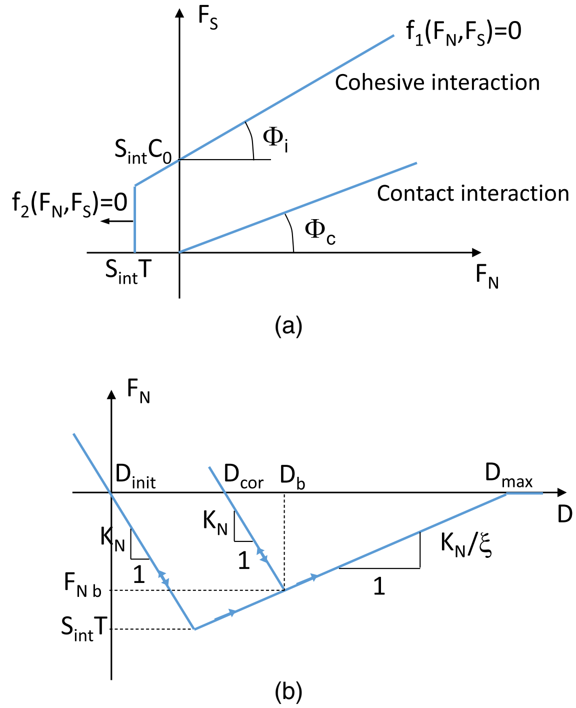

Fig. 7. Interaction laws in (a) tangential and (b) normal directions

where F_n and F_s = normal and shear forces related to stress quantities C_o (cohesion) and T (local tensile limit), respectively; Φ_i = frictional angle.

These constitutive behavior parameters are identified (in a similar way as for E and ν) from macroscopic properties such as the compressive and tensile strengths σ_c and σ_t, and the fracture energy G_f. A softening factor ξ (which must be identified) is introduced in tension to make the tensile effort tend progressively to zero (Hentz 2003). A maximum interaction distance $D_{\max}$ and the postpeak force are defined as follows:

$$D_{\max} = D_{\text{init}} + (1+\xi)\frac{S_{\text{int}}T}{K_n} \tag{4}$$

$$F_n = \frac{K_n}{\xi}(D^b - D_{\max}) \tag{5}$$

where D_{init} and D^b = initial and actual distances between the involved elements.

After the loss of cohesion at $D = D_{\max}$, the cohesive (or linked) interaction becomes a contact interaction modeled by means of a classical Coulomb friction model characterized by a friction angle Φ_c (Fig. 7).

A priori, friction angles Φ_i and Φ_c are independent because contact friction is related to the roughness of the contacting surfaces, whereas cohesive friction is related to the cohesive properties of the material. The DE model considered herein does not represent the material at the mesoscale, but seeks to reproduce the macroscopic behavior of concrete. Thus, these friction angles must be identified separately, as suggested in Camborde et al. (2000).

Compression Test Simulation

To identify the constitutive behavior parameters, a compression test was simulated with $\sigma_c = 33$ MPa, $E = 30$ GPa, and $\nu = 0.21$ (Gabet 2006; Gabet et al. 2006) using the DE sample shown in Fig. 1. No numerical damping was applied. This simulation

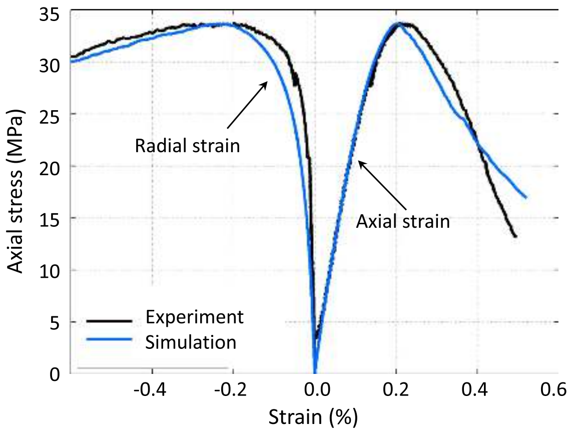

Fig. 8. Simulation of a compression test

made it possible to identify C_o, ξ (Fig. 8). This compression test is unsuitable for identifying the local tensile strength T because this parameter only exerts a slight influence on the compression test simulation.

Brazilian Test Simulation

The Brazilian indirect tensile test (Carneiro 1943; Fig. 9) serves to identify the local tensile strength T. In the simulation performed, DEM was applied to model the cylindrical concrete specimen (diameter of 16 cm, length of 32 cm), and the two wooden bearing strips were represented through a conventional finite element (FE) model (Fig. 10).

The following DE model parameters were used: $E = 25$ GPa, $\nu = 0.16$, $T = 2.3$ MPa, $C_0 = 4.5$ MPa, $\Phi_i = 15°$, $\Phi_c = 15°$, $\xi = 5$. Fig. 11 shows the horizontal displacement, U_x, of the DE specimen once it has been split into two half-cylinders, as would be expected for this brittle fracture test in which a vertical crack is generated as shown in the figure by a dashed white line. Because of vertical compressive loading, the tensile state occurs perpendicular to the loading plane, which in turn causes the specimen to split. A sharp basic color change in the horizontal direction in Fig. 11 reveals creation of two half-cylinder blocks moving in opposite directions.

To quantify the specimen response, the tensile stress at the specimen center is calculated using the well-known formula, $\sigma_t = 2P/\pi dL$, with P being the resultant vertical force applied by bearing strips on the specimen and d and L being the specimen diameter and length, respectively. The calculated tensile strength of 3.4 MPa is in good agreement with the experimental value of 3.3 MPa (Fig. 12). A dynamic resolution algorithm is used. To be sure that the applied velocity is small and the calculation reproduces quasi-static conditions correctly, it is verified a posteriori that the kinetic energy is small compared with the deformation energy.

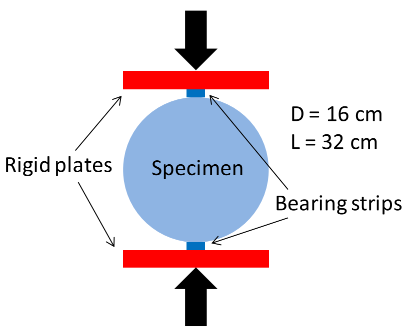

Fig. 9. Brazilian indirect tensile test setup

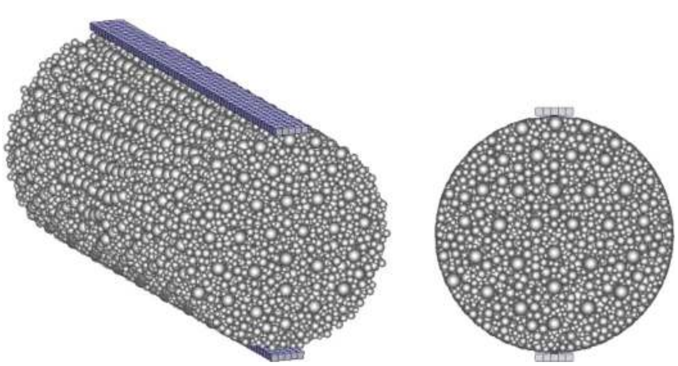

Fig. 10. Mixed DE-FE mesh for the Brazilian test

Nooru-Mohamed Multiaxial Test Simulation

The Nooru-Mohamed test (Nooru-Mohamed 1992) was simulated in order to qualitatively validate the DEM for its description of damage in a double-edge notched specimen subjected to a successive combination of shear and tension (Fig. 13).

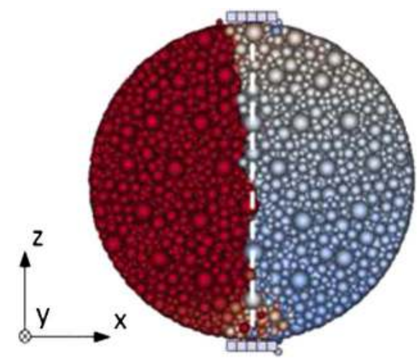

Fig. 11. U_x displacement field after splitting

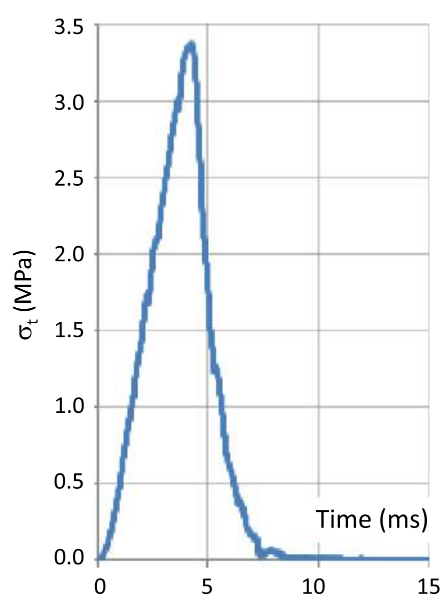

Fig. 12. Calculated tensile strength σ_t

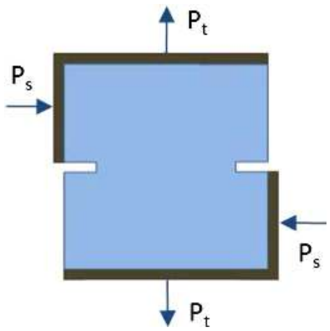

Fig. 13. Schematic of the Nooru-Mohamed test

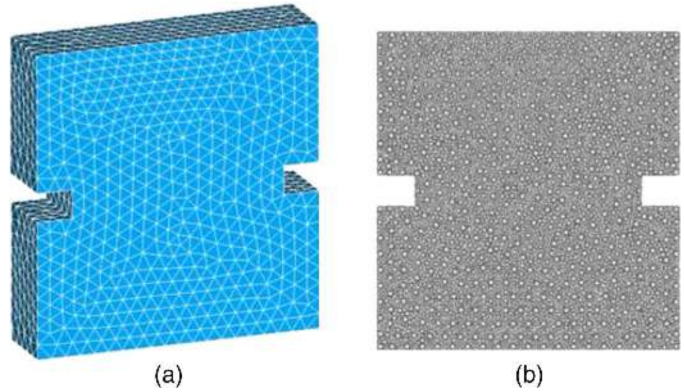

Fig. 15. (a) Tetrahedra and (b) DE meshes for the Nooru-Mohamed test simulation

First of all, the specimen was loaded by an increasing shear force P_s while maintaining the normal force P_t equal to zero. After reaching a certain load level, the force P_s was held constant and the specimen was subjected to an increasing normal displacement. Three values of shear force were considered: $P_s = 5$ kN, $P_s = 10$ kN, and $P_s = 27.5$ kN, with the last value being the maximum shear force the specimen was able to withstand. In all cases, the failure pattern consisted of two macroscopic cracks propagating from the notches in an inclined direction. For the lowest shear force value, these cracks were nearly horizontal and close to each other whereas for the highest value they were highly curved (Fig. 14, adapted from Nooru-Mohamed 1992).

The specimen used for the DE simulation had the same dimensions as in the test, except for the slightly greater notch width used because the *SpherePadder++* algorithm cannot deal for the moment with very narrow notches. This modification exerted no influence on the crack path, which solely depends on the P_s/P_t ratio. The initial tetrahedra and final DE meshes are shown in Fig. 15. The following DE model parameters were used: $E = 29$ GPa, $\nu = 0.2$, $T = 3$ MPa, $C_0 = 6$ MPa, $\Phi_i = 15°$, $\Phi_c = 15°$, $\xi = 5$.

The crack path's output by the *EUROPLEXUS* calculation (Fig. 16) can be compared with the experimental results (Fig. 14) for three shear force values. For the three loading paths, the numerical crack path predictions are in a very good agreement with experimental results. Even the highly curved cracks generated by the highest load level have been reproduced accurately. For each DE, damage is defined as a ratio of remaining cohesive links over the initial number of links; thus, it can be used only as an indicator for material degradation and cannot indicate definitively the presence of a macrocrack. To ensure that the damage state displayed in Fig. 16(a) corresponds to a real discontinuity, the vertical displacement field of the DE specimen was drawn [Fig. 16(b)]. The basic color changes in the vertical direction reveal the presence of two macrocracks going through the specimen. Dashed white lines depict experimental crack patterns.

The force-displacement (f-u) diagram is not shown here because it is difficult to obtain for this particular case. Indeed, to generate tension in the DE model of the specimen, two zones have been defined at the upper and lower sides (horizontal black lines in Fig. 13), and linearly increasing vertical displacements have been imposed on discrete elements whose centers were situated in these zones. Thus, to obtain the resulting force for the f-u diagram, it is necessary to sum up the vertical projections of all interelement forces (normal and tangential components of cohesive links) crossing the complex separation surface [because of polydisperse DE graining as shown Fig. 15(b)] between these zones and the rest of the specimen.

An accurate description of damage and cracks pattern in the Brazilian and Nooru-Mohamed tests validates the proposed approach to modeling concrete behavior under static loading.

Steel-Concrete Bond Modeling

General Presentation

The modeling of reinforced concrete structures requires accounting for steel reinforcement and its interaction with concrete. It is possible to model rebars in a DEM framework by using aligned discrete elements and special beam-like connections, as proposed in Rousseau (2009). However, because of the complex grid patterns of rebars used in actual engineering structures, the application of a DEM-type model for steel is inconvenient for many reasons,

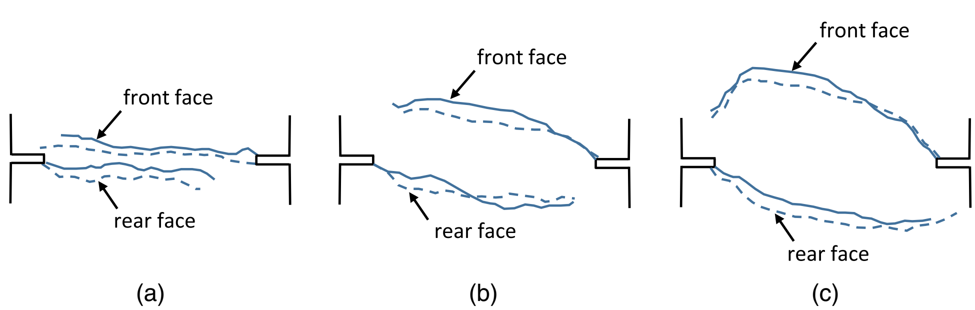

Fig. 14. Crack patterns for three different shear load values: (a) $P_s = 5$ kN; (b) $P_s = 10$ kN; (c) $P_s = 27.7$ kN (adapted from Nooru-Mohamed 1992)

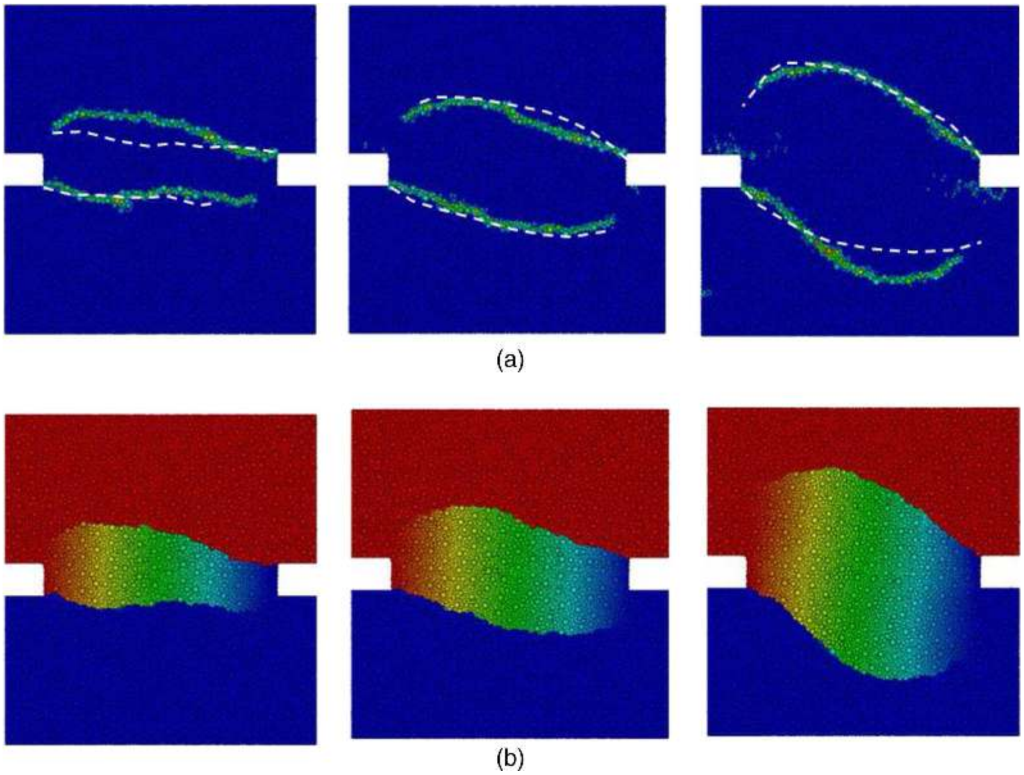

Fig. 16. (a) Crack patterns and (b) vertical displacement calculated for three shear load values

including complicated mesh construction and poor numerical performance owing to the small size of discrete rebar elements. In this study, the steel reinforcement was modeled through a conventional FEM with beam-like elements; also, a new steel-concrete bond model is proposed to appropriately link concrete spherical discrete elements with FE rebar (Masurel 2015).

In the proposed computational framework, the steel-concrete (S-C) interface has been modeled as a set of links established between a given rebar and the concrete discrete elements located in the vicinity of the rebar (Fig. 17). Consequently, for a given mn rebar finite element, S-C links are created for the concrete discrete elements (shading in Fig. 17) that feature an orthogonal projection on this rebar element; their centers lie within an interaction zone whose radius (referred to as the interaction distance, D_{int}) is proportional to the rebar radius R_a, with λ_a as the proportionality coefficient. To determine the value of this coefficient, the procedure suggested in the literature (Torre-Casanova 2012) is applied, relying on a series of simulations of the pull-out test by varying the

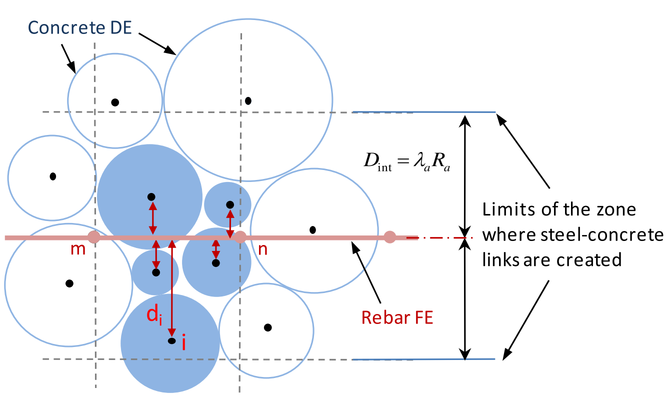

Fig. 17. Schematic representation of steel-concrete links

interaction coefficient in order to match the numerical response with the imposed S-C tangential law.

Each S-C link can be symbolically represented as shown in Fig. 18(a). This representation is equivalent to two independent nonlinear springs: one normal, the other tangential. The behavior of the normal spring is assumed to be brittle in tension and elastic-plastic in compression [Fig. 18(c)]. The tangential behavior [Fig. 18(b)] is devised to reproduce the response of the S-C bond observed in pull-out tests; this response differs for high-strength ribbed rebar and smooth rebar.

The key point of this S-C bond model is that its normal and tangential components remain independent. For the normal component, the restoring force [Eq. (6)] is calculated at each time step from the variation in distance between the concrete DE center and its orthogonal projection (point P_N) on the corresponding rebar element:

$$F_N = -K_N(h^n - h^0) \tag{6}$$

Because point P_N is fictitious, the calculated restoring force is logically redistributed on the nodes of the given rebar beam element. The calculation remains the same as in the case of extensive sliding, where the concrete DE is projected onto the neighboring rebar element [Fig. 19(a)]. The normal component forces are always in equilibrium for both translation and rotation.

For the tangential component, another projection point P_S is defined. As opposed to P_N, which can slide along the rebar, P_S does not move from its initial position on the rebar element. The restoring force [Eq. (7)] for the tangential spring is proportional to the distance between P_N and P_S:

$$F_S = -K_S u_S \tag{7}$$

As for the normal component, the force F_S is distributed on the nodes of the rebar element, where point P_N is also projected.

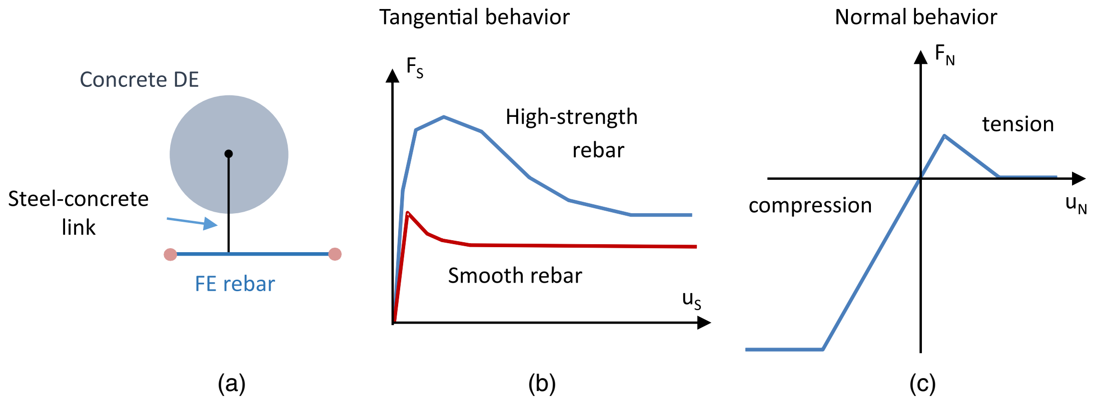

Fig. 18. Representation of the (a) S-C link and its interaction laws in both the (b) tangential and (c) normal directions

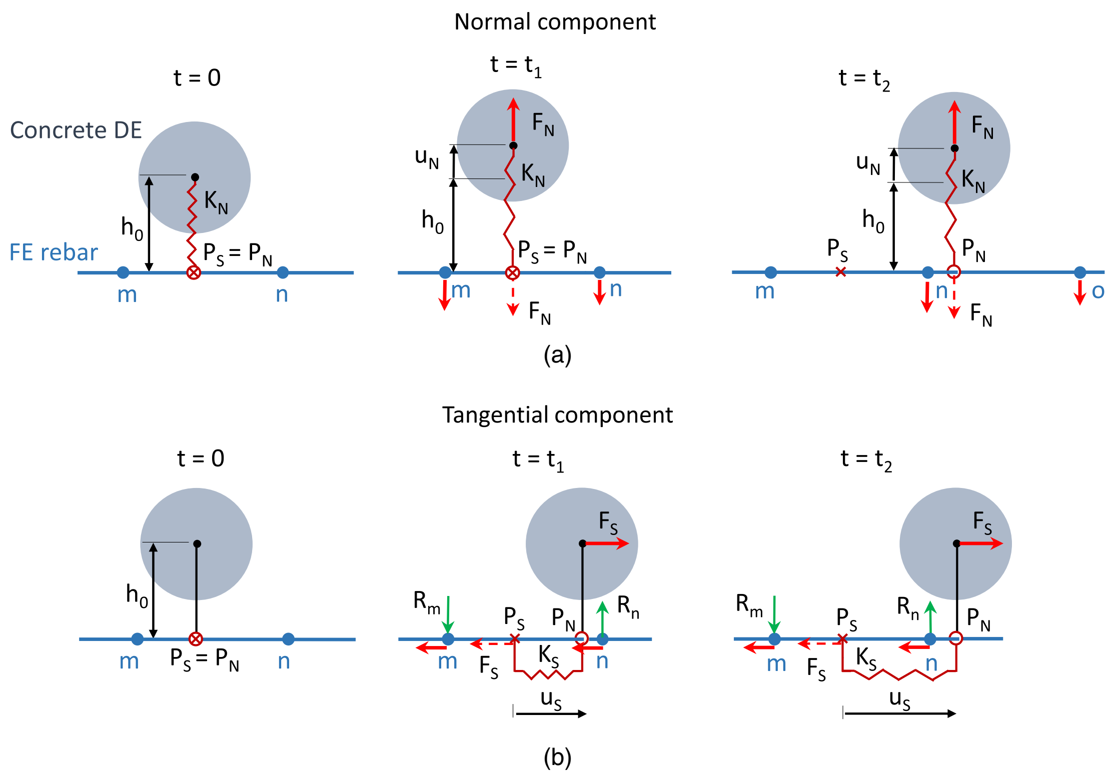

Fig. 19. (a) Normal and (b) tangential behavior in the event of significant sliding

The tangential forces are balanced in translation but not in rotation, which can generate model instabilities. To respect rotation equilibrium, two vertical reaction forces R_m and R_n [green arrows in Fig. 19(b)] are calculated from Newton's second law for rotation and then applied to the nodes of the considered rebar element.

The interaction laws for the normal and tangential components of the proposed bond model were adequately implemented into the *EUROPLEXUS* fast dynamics software; moreover, verification tests were performed in loading-unloading regimes to ensure that the prescribed laws (Fig. 18) were respected during complex loading paths (Fig. 20). As can be observed, the normal and tangential stiffnesses (curve slopes) of the bond components vary in an appropriate manner with respect to hardening and softening regimes—namely, the slope decreases in the softening regime and the envelope curve (Fig. 18) is systematically reached as the displacement increases.

For the moment, the tangential behavior is completely independent of what happens in the normal direction. This corresponds to the situation that typically occurs in standard (unconfined) pull-out tests, where mainly tangential behavior is involved. To couple normal and tangential responses, the actual model has to be completed and calibrated on confined pull-out tests.

Steel-Concrete Tie in Tension

To test the capability of the mixed DE/FE model to reproduce the cracking of reinforced concrete, the simple model case of a steel-concrete tie in tension is considered (Fig. 21). According to this case, as fully described in Torre-Casanova (2012), the loading is applied symmetrically at the ends of a single reinforcing rod embedded in a concrete column, and the S-C interface is directly involved in load transmission between the steel and the concrete.

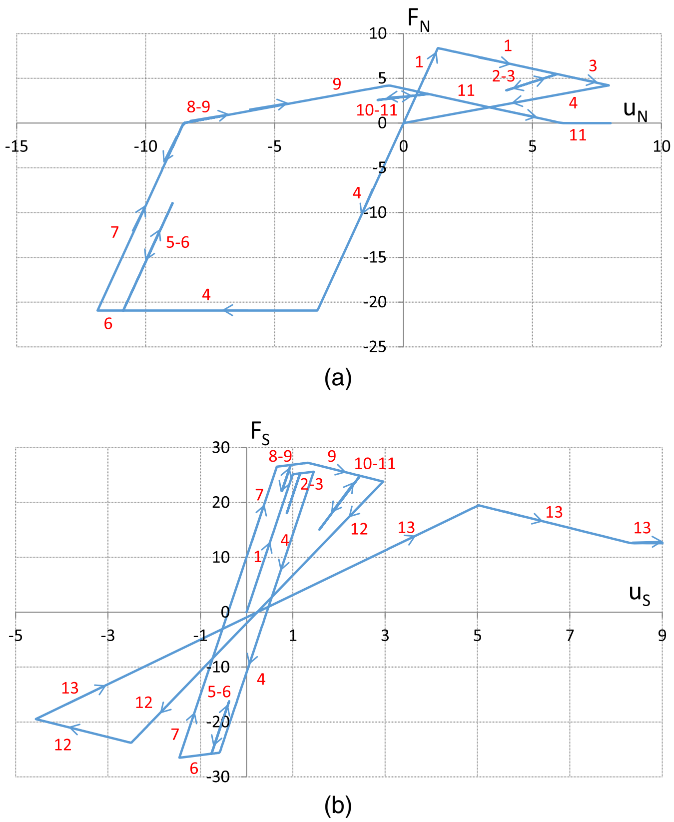

Fig. 20. (a) Normal and (b) tangential behavior during a loading-unloading regime

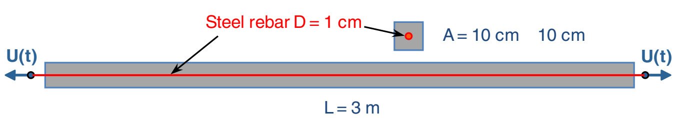

Fig. 21. Schematic representation of the studied steel-concrete tie

Standard material properties are adopted for the steel ($E = 210$ GPa, $\nu = 0.3$) and concrete ($E = 30$ GPa, $\nu = 0.2$, $T = 2$ MPa, $C_0 = 6$ MPa, $\Phi_i = 15°$, $\Phi_c = 15°$, $\xi = 5$) of this tie.

Fig. 22(a) shows the damage state of the tie when the cracking process is completely stabilized (no more new transverse cracks appear). A finite number of cracks is generated, which is in agreement with the experimental results found during the tie tensile tests (Farra and Jaccoud 1993). By comparing tensile stress in the rebar [Figs. 22(b) and 23] with the final damage state of the concrete, it can be seen that plastic flow occurs in the rebar sections in front of the formed cracks. These cracks separate the concrete fragments with uniform longitudinal displacements, as indicated by the basic color changes in Fig. 22(c). Relative sliding of the rebar with respect to the surrounding fragmented concrete can be seen in Fig. 24.

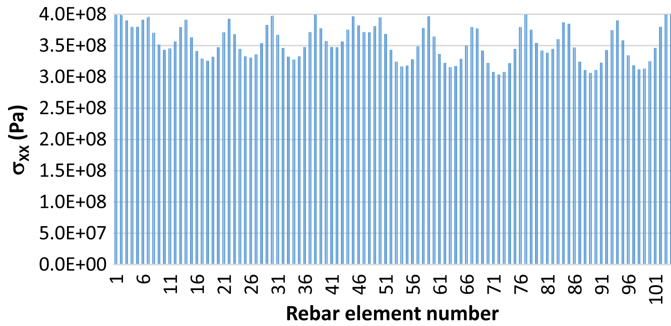

Fig. 23. Tensile stress in the rebar

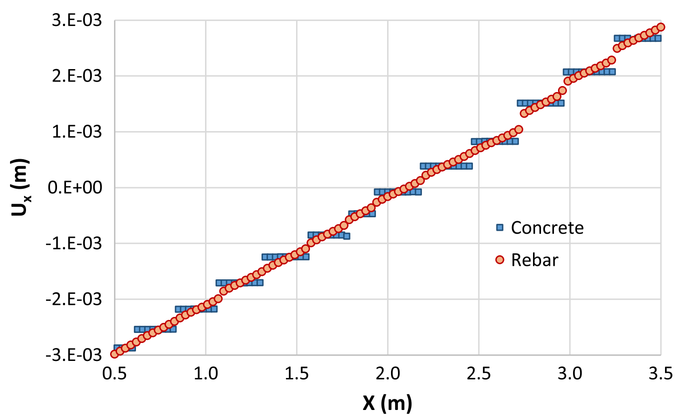

Fig. 24. Longitudinal displacements in the concrete and the rebar

These first results show that the proposed mixed DEM/FEM model ensures an effective load transmission between the rebar model and the concrete model, in obtaining a realistic distribution of force and damage along the rebar. Work is in progress to study the capability of this approach to represent the effect of the reinforcement ratio on the crack spacing.

Hard Impact on a RC Beam

To demonstrate the modeling capability of the proposed numerical approach, a low-velocity hard-type impact on a reinforced concrete beam is simulated and numerical results are compared with measured data obtained on a CEA Orion drop tower (Chambart 2009).

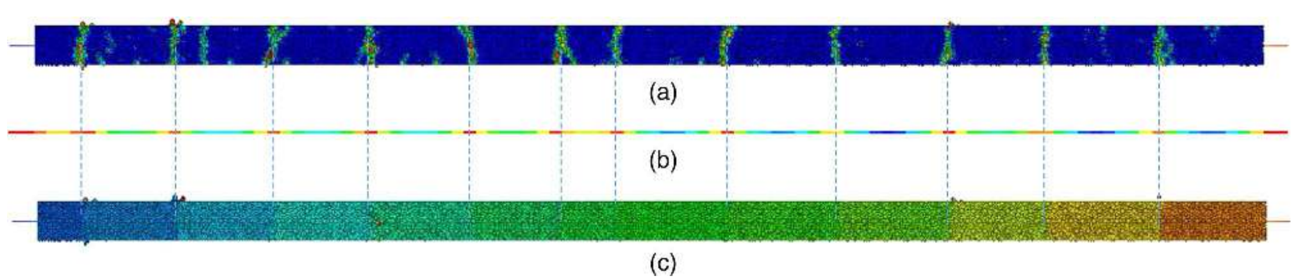

Fig. 22. (a) Damage state of the concrete; (b) tensile stress in the rebar; (c) U_x displacement of the concrete

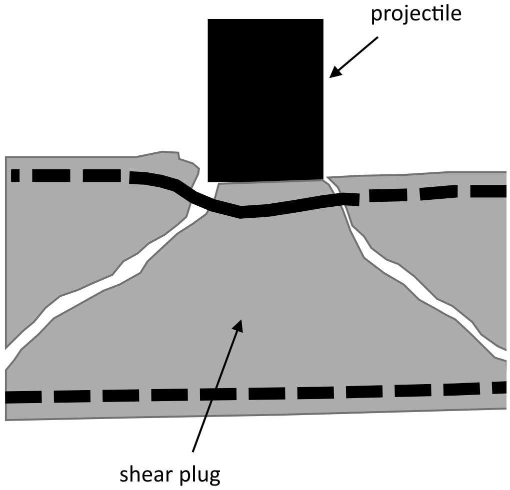

Fig. 25. Experimentally observed shear-type failure mode (adapted from Chambart 2009)

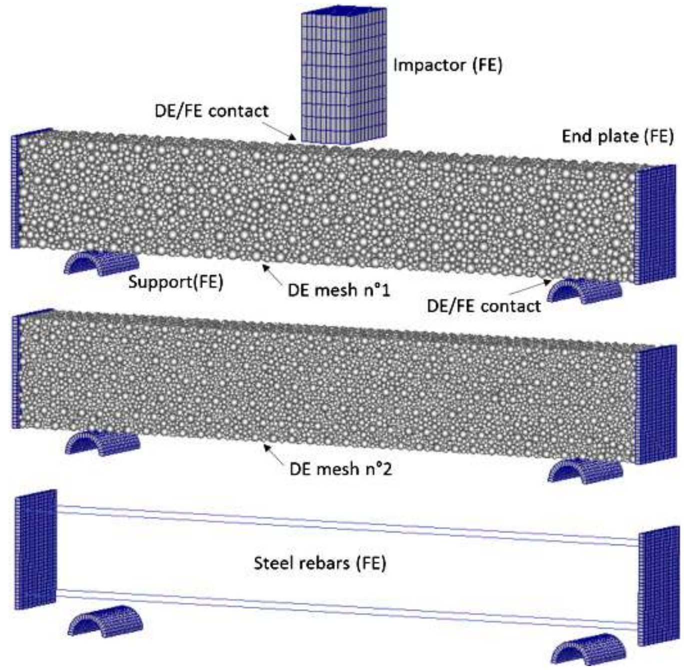

Fig. 26. View of the DEM/FEM model with coarse and fine DE meshes

A short concrete beam of 1.3-m length with a rectangular cross section (height 0.2 m and width 0.15 m) is considered. The beam is made of ordinary concrete with a compressive strength of 33 MPa. It is doubly reinforced with two 12-mm-diameter ribbed high-yield steel rebars at the bottom of the beam and two 8-mm-diameter ribbed high-yield steel rebars at the beam's top. The rebars are welded to 1-cm-thick steel plates disposed at the beams' ends to avoid excessive sliding between the rebars and the concrete during deformation and cracking. Two steel semicircular cylinders support the beam and form the 1-m span. To avoid rebound on the supports, the beam is held by two steel frames. Impact loading is generated by a 103.65-kg mass dropped from a height of 3.5 m directly onto the beam with an impact velocity of 8.3 m/s. In this hard impact case, a characteristic conical shear plug delimited by oblique cracks is generated (Fig. 25) but the longitudinal rebars are not broken.

A detailed mixed DE/FE numerical model of the experimental device is built (Fig. 26): the concrete is represented by DE formulation, whereas FEM is used to model the bending steel reinforcement, the end plates, the semicircular cylindrical supports, the steel frames (not shown in the figure), and the impactor. Unilateral contact conditions are prescribed everywhere between the DE and FE parts of the model. Steel-concrete bond laws presented previously are applied to describe the interaction between the concrete and the steel reinforcement. Pull-out tests for 8- and 12-mm ribbed high-yield steel rebars were realized to characterize the tangential laws of the model. To study the influence of discretization refinement of the concrete on the whole response of the model, two different DE meshes are built. The DE Mesh n°1 shown in Fig. 26 contains 24.677 DE elements ($R_{\max} = 1.05$ cm, $R_{\min} = 3.5$ mm), whereas Mesh n°2 is finer and contains 55.690 DE with $R_{\max} = 7.9$ mm, $R_{\min} = 2.6$ mm.

To take into account the increased resistance of the concrete under high rate loading, the local strain-rate dependency (through a bilinear law proposed in Hentz 2003) is introduced in the model, enabling it to correctly reproduce the experimental strain-rate sensitivity. Infinite impulse response filtering is applied to the velocity before calculating the strain rate.

Fig. 27 shows the damage pattern, after the projectile rebound, obtained in the simulations with two DE meshes considered. In the absence of shear reinforcement, a shear plug is formed under the impactor, with the angle of the plug in conformity with the experimental observation (Fig. 25).

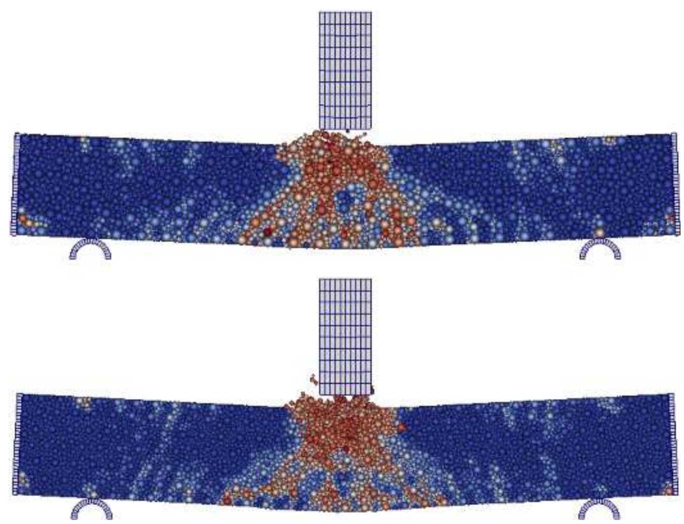

Fig. 27. Final damage state obtained with the coarse and fine DE meshes

Because the diffuse damage state is difficult to interpret in terms of macrocracking, a special algorithm has been developed to detect fragments in the DE concrete model. This algorithm helps make visible material discontinuities between the DE blocks created in the simulation with no common links left. These discontinuities correspond to sharp color changes in Fig. 28. As can be seen, the damaged zone is limited by oblique cracks as observed in the experiment.

The time evolution of deflection of the beam is shown in Fig. 29. The calculated residual U_y displacement is very close to the 24-mm displacement measured in the experiment. These global-type

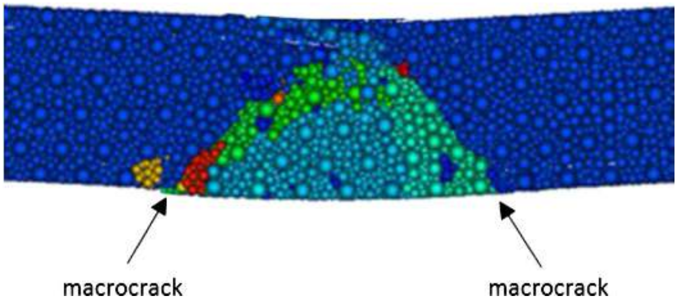

Fig. 28. Concrete fragments detected in the calculation with the coarse mesh

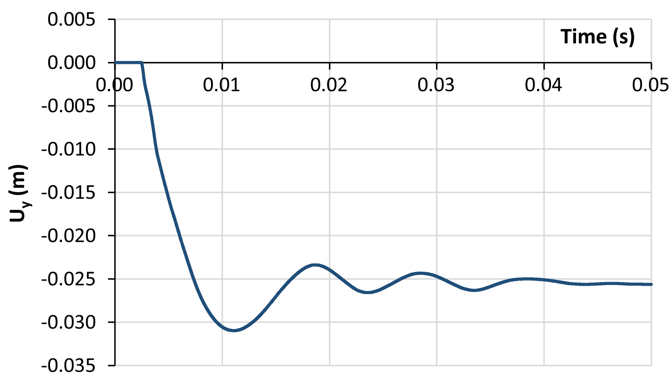

Fig. 29. Deflection predicted in the calculation with the coarse mesh

results show that the model dissipates the right amount of energy injected into the beam by the impactor.

Conclusion

An original mixed DEM/FEM approach was proposed to model the advanced damage states of reinforced concrete structures subjected to severe accidental-type loads. This model is based on a discrete-element modeling of concrete, which yields a very natural representation of both the undamaged cohesive behavior of concrete and its cracking and fracturing processes during the final stages of deformation. In order to master the DEM modeling of concrete, an extensive numerical study was conducted to determine the minimum discretization needed for a DEM sample to reproduce the macroscopic behavior of concrete. The standard finite-element method was applied to represent steel reinforcement through an elastic-plastic beam model. This setup accounts for the arbitrary complex grid patterns of rebars used in actual engineering structures. To complete this modeling framework, an original steel-concrete bond model was developed; its normal and tangential responses were effectively decoupled and could be treated independently with a suitable fitting on the available experimental data. The material parameters of this novel approach were identified by simulating both the compression test and the Brazilian indirect tension test. An accurate description of the damage phenomena (damage pattern and curved cracks) in the simulation of the complex Nooru-Mohamed shear-tension test validated the proposed approach to modeling concrete behavior. The entire approach was then applied to simulate a steel-concrete tie in tension. A realistic cracking process and suitable load transmission between the rebar model and the concrete model were predicted. Lastly, the mixed DEM-FEM model was applied to simulate the advanced damage state of a RC beam under a hard-type impact. The crack pattern predicted by the calculation was in general accordance with the experiment. The global nonlinear response of the RC structure was also correctly predicted—namely, the beam deflection.

The whole DEM/FEM computational framework presented in this study runs on parallel computers, and it is now ready for use in simulating the static and dynamic responses of industrial-size reinforced concrete structures.

Acknowledgments

The authors gratefully acknowledge the financial support (contract no. 2011/1105) provided by the French National Research and Technology Association (ANRT).

References

Belytschko, T., and Lin, J. I. (1987). “A three-dimensional impact-penetration algorithm with erosion.” *Comput. Struct.*, 25(1), 95–104.

Camborde, F., Mariotti, C., and Donzé, F. V. (2000). “Numerical study of rock and concrete behavior by discrete element modeling.” *Comput. Geotech.*, 27(4), 225–247.

Carneiro, F. L. L. B. (1943). “A new method to determine the tensile strength of concrete.” *Proc., 5th Meeting of the Brazilian Association for Technical Rules (“Associação Brasileire de Normas Técnicas—ABNT”)*, 126–129 (in Portuguese).

Chambart, M. (2009). “Endommagement anisotrope et comportement dynamique des structures en béton armé jusqu’à la ruine [Anisotropic damage and dynamic behavior of reinforced concrete structures until failure].” Ph.D. thesis, Ecole normale supérieure de Cachan (ENS Cachan), Cachan Cedex, France (in French).

Cusatis, G., Pelessone, D., and Mencarelli, A. (2011). “Lattice discrete particle model (LDPM) for failure behavior of concrete. I: Theory.” *Cem. Concr. Compos.*, 33(9), 881–890.

EUROPLEXUS [Computer software]. ⟨http://www-epx.cea.fr⟩.

Farra, B., and Jaccoud, J. P. (1993). “Influence du béton et de l’armature sur la fissuration des structures en béton [Influence of concrete and reinforcement on cracking of concrete structures].” *Rapport des essais de tirants sous déformation imposée de courte durée [Rep. on Experiments on Ties under an Imposed Strain of Short Duration]*, EPF de Lausanne, Lausanne, Switzerland (in French).

Gabet, T. (2006). “Comportement triaxial du béton sous fortes contraintes: Influence du trajet de chargement [Triaxial behavior of concrete under strong stresses: Influence of the loading path].” Ph.D. thesis, Université de Grenoble, Saint-Martin-d'Hères, France (in French).

Gabet, T., Vu, X. H., Malecot, Y., and Daudeville, L. (2006). “A new experimental technique for the analysis of concrete under high triaxial loading.” *J. Phys. IV*, 134, 635–640.

Hentz, S. (2003). “Modélisation d’une Structure en Béton Armé Soumise à un Choc par la méthode des Éléments Discrets [Modeling of a structure in reinforced concrete submitted to a choc by the discrete element method].” Ph.D. thesis, Université de Grenoble, Saint-Martin-d'Hères, France (in French).

Hentz, S., Daudeville, L., and Donzé, F. V. (2004a). “Discrete element modelling of concrete submitted to dynamic loading at high strain rate.” *Comput. Struct.*, 82(29–30), 2509–2524.

Hentz, S., Daudeville, L., and Donzé, F. V. (2004b). “Identification and validation of a discrete element model for concrete.” *J. Eng. Mech*, 10.1061/(ASCE)0733-9399(2004)130:6(709), 709–719.

Jerier, J.-F., Richefeu, V., Imbault, D., and Donzé, F. V. (2010). “Packing spherical discrete elements for large scale simulations.” *Comput. Methods Appl. Mech. Eng*, 199(25–28), 1668–1676.

Liu, G. R. (2010). *Meshfree methods: Moving beyond the finite element method*, 2nd Ed., CRC Press, Boca Raton, FL.

Masurel, A. (2015). “Modélisation mixte éléments discrets/éléments finis de la dégradation de structures en béton armé sous impact sévère

[Mixed discrete element/finite element modeling of degradation of reinforced concrete structures under severe impact]." Ph.D. thesis, Université de Grenoble Alpes, Saint-Martin-d'Hères, France (in French).
Nguyen, V. P., Rabczuk, T., Bordas, S., and Duflot, M. (2008). "Meshless methods: A review and computer implementation aspects." *Math. Comput. Simul.*, 79(3), 763–813.
Nooru-Mohamed, M. B. (1992). "Mixed-mode fracture of concrete: An experimental approach." Ph.D. thesis, Delft Univ. of Technology, Delft, Netherlands.
Prado, E., and Van Mier, J. (2003). "Effect of particle structure on mode I fracture process in concrete." *Eng. Fract. Mech.*, 70(14), 1793–1807.
Rousseau, J. (2009). "Modélisation numérique du comportement dynamique de structures sous impact sévère avec un couplage éléments discrets / éléments finis [Numerical modeling of dynamic behavior of reinforced concrete structures under severe impact using DEM/FEM coupling]." Ph.D. thesis, Université de Grenoble, Saint-Martin-d'Hères, France (in French).
Rousseau, J., Frangin, E., Marin, P., and Daudeville, L. (2008). "Damage prediction in the vicinity of an impact on a concrete structure: A combined FEM/DEM approach." *Comput. Concr.*, 5(4), 343–358.
Rousseau, J., Frangin, E., Marin, P., and Daudeville, L. (2009). "Multidomain finite and discrete elements method for impact analysis of a concrete structure." *Eng. Struct.*, 31(11), 2735–2743.
SALOME [Computer software]. ⟨http://www.salome-platform.org/⟩.
SpherePadder++ [Computer software]. ⟨https://subversion.assembla.com/svn/spherepadder/trunk⟩.
Torre-Casanova, A. (2012). "Account for steel-concrete bond in simulation of industrial structures." Ph.D. thesis, Ecole Normale Supérieure de Cachan, Cachan Cedex, France (in French).